

Research Paper

Fabrication of Tissue-Engineered Bionic Urethra Using Cell Sheet Technology and Labeling By Ultrasmall Superparamagnetic Iron Oxide for Full-Thickness Urethral Reconstruction

Shukui Zhou¹, Ranxin Yang¹, Qingsong Zou¹, Kaile Zhang¹, Ting Yin², Weixin Zhao³, Joseph G. Shapter⁴, Guo Gao²✉, Qiang Fu¹✉

1. Department of Urology, Affiliated Sixth People's Hospital, Shanghai Jiao Tong University, Shanghai, China;
2. Institute of Nano Biomedicine and Engineering, Department of Instrument Science and Technology, School of Electronic Information and Electrical Engineering, Shanghai Jiao Tong University, Shanghai, China;
3. Wake Forest Institute for Regenerative Medicine, Winston Salem, NC, USA;
4. School of Chemical and Physical Sciences, Flinders University, Bedford Park, Adelaide 5042, Australia.

✉ Corresponding authors: Qiang Fu, Department of Urology, Affiliated Sixth People's Hospital, Shanghai Jiao Tong University, Shanghai, China. ZIP: 200233. Fax: 021-63868708, E-mail address: jamesqfu@aliyun.com (Q. Fu). Guo Gao, E-mail address: guogao@sjtu.edu.cn (G. Gao).

© Ivyspring International Publisher. This is an open access article distributed under the terms of the Creative Commons Attribution (CC BY-NC) license (<https://creativecommons.org/licenses/by-nc/4.0/>). See <http://ivyspring.com/terms> for full terms and conditions.

Received: 2016.12.20; Accepted: 2017.04.21; Published: 2017.06.25

Abstract

Urethral strictures remain a reconstructive challenge, due to less than satisfactory outcomes and high incidence of stricture recurrence. An "ideal" urethral reconstruction should establish similar architecture and function as the original urethral wall. We fabricated a novel tissue-engineered bionic urethras using cell sheet technology and report their viability in a canine model. Small amounts of oral and adipose tissues were harvested, and adipose-derived stem cells, oral mucosal epithelial cells, and oral mucosal fibroblasts were isolated and used to prepare cell sheets. The cell sheets were hierarchically tubularized to form 3-layer tissue-engineered urethras and labeled by ultrasmall super-paramagnetic iron oxide (USPIO). The constructed tissue-engineered urethras were transplanted subcutaneously for 3 weeks to promote the revascularization and biomechanical strength of the implant. Then, 2 cm length of the tubularized penile urethra was replaced by tissue-engineered bionic urethra. At 3 months of urethral replacement, USPIO-labeled tissue-engineered bionic urethra can be effectively detected by MRI at the transplant site. Histologically, the retrieved bionic urethras still displayed 3 layers, including an epithelial layer, a fibrous layer, and a myoblast layer. Three weeks after subcutaneous transplantation, immunofluorescence analysis showed the density of blood vessels in bionic urethra was significantly increased following the initial establishment of the constructs and was further up-regulated at 3 months after urethral replacement and was close to normal level in urethral tissue. Our study is the first to experimentally demonstrate 3-layer tissue-engineered urethras can be established using cell sheet technology and can promote the regeneration of structural and functional urethras similar to normal urethra.

Key words: tissue engineering; cell sheet technology; bionic urethra; urethral reconstruction; transplant imaging; ultrasmall super-paramagnetic iron oxide (USPIO).

Introduction

Urethral defects or strictures have a variety of causes and are still challenging issues in urology. The foreskin flap, scrotum flap, oral mucosa, or colonic mucosa are usually used for urethroplasty, and many reports have demonstrated good results after the procedure [1, 2]. However, their use can lead to

several complications associated with the mode of sacrificing healthy tissue to repair worn tissue, e.g., large tissue defects at the donor sites, long-term changes in speech, hair growth, graft contraction, urethrostenosis, lithogenesis, and formation of a urethral diverticulum [3, 4]. Moreover, multilayer

structures rather than a single structure are commonly destroyed in urethral defects or strictures, including the epithelial, fibrous, and muscular layers, thus it is challenging to provide autologous tissue with similar structures, form, and function for the “ideal” repair of urethral strictures. The rapid development of tissue engineering techniques provides an effective way to treat urethral defects and urethral strictures [5, 6].

Recently, cell sheet technology has been widely used in the field of tissue engineering. A cell sheet is composed of cells and extracellular matrix (ECM). Compared with the traditional composition of cells and scaffold materials, cell sheets feature an increased concentration of cells, more uniform cell distribution, and the absence of immunological interference caused by scaffold materials. Takeuchi *et al.* [7] reported that cell sheet transplantation consistently yielded greater cell survival for up to 12 months compared with cell injection, and a smaller number of apoptotic cells were present in the cell sheets than in the cell suspensions. Moreover, the 3-dimensional structure of the ECM in cell sheets provides a nutritive and structural microenvironment for cell adhesion and growth, as well as regulating homeostasis, differentiation, and regeneration. Cell sheets can adhere tightly to host tissues or adhere to each other for abundant ECM in cell sheets, which helps build multilayer cell sheets for soft tissue repair. In previous studies, various types of 3-D soft tissues without scaffolds were fabricated using cell sheet stacking technology [8-10]. The urethra is a single tubular structure and also is a type of soft tissue. The urethral histological structure involves mucosa, submucosa, and muscularis (from the inside to the outside). Nonetheless, to the best of our knowledge, there have been no reports about the use of cell sheet technology to establish a 3-layer tissue-engineered urethra, and whether such a construct can be applied for urethral repair and replacement is still unclear.

After the transplantation of cell sheets, monitoring the distribution, proliferation, and migration of the transplanted cells in the body is one of the most important aspects in identifying the mechanisms by which seed cells exert their effects. However, the traditional research methods for histological analysis can be performed only *in vitro*, which is slow, time-consuming, and invasive. Magnetic resonance imaging (MRI) offers innovative and high-resolution approaches to dynamically and persistently detect a small fraction of labeled cells *in vitro* and *in vivo*, and thus it can be used as an ideal tracer method. Ultrasmall superparamagnetic iron oxide (USPIO) consists of nanoscale iron particles where the particle size is <50 nm [11]. Many studies have shown labeling with optimized USPIO doses not

trigger apoptosis or impair cell survival and proliferation capacity [12-14]. From early reports, USPIO has been proven to be an excellent MRI contrast agent for detecting cells and scaffolds *in vitro* and *in vivo* [12, 15, 16]. Recently, our experiments confirmed USPIO with the optimal concentration of 50 µg Fe/mL could be used for *in vivo* labeling of the Adipose-derived stem cells (ADSCs) sheets for at least 12 weeks [17].

Oral mucosal wounds are characterized by rapid reorganization and re-epithelialization, and oral keratinocytes have been used to demonstrate the feasibility of repairing urethral defects. Oral mucosal harvesting is convenient and safe, and only a small amount of tissue can yield enough oral mucosal epithelial cells and oral fibroblasts for therapeutic applications. Because they reside in a physiological environment similar to that of urinary tract epithelium, oral keratinocytes have the transdifferential potential toward the uroepithelium in a urological environment [18]. In contrast, muscle cells harvested from muscle biopsy involve donor site morbidity, and the biopsy procedure is painful and generally requires large muscle biopsies to obtain sufficient muscle cells. ADSCs are the most common stem cell type to be applied in autoplasmic transplantation and possess the powerful property of multidirectional differentiation and reproductive activity. In earlier experiments, ADSCs were induced into myoblasts with 5-azacytidine *in vitro* and were used successfully by our group to treat stress urinary incontinence using cell suspension injection [19]. In the present study, guided by the histologic features of the urethra, we chose different sources of seed cells (ADSCs, oral mucosal epithelial cells, and oral mucosal fibroblasts) to build the corresponding cell sheets and labeled cells using USPIO at optimized dosages. Then we investigated the feasibility of constructing tissue-engineered bionic urethras using cell sheet technology for full-thickness urethral repair and reconstruction.

Materials & methods

Materials

5-Azacytidine and collagenase type I were purchased from Sigma (St. Louis, MO, USA). Desmin, α-SMA, PAX7, CD34 monoclonal antibodies, and rabbit anti-mouse FITC tags were obtained from Abcam (Cambridge, MA, USA). Cell culture products and reagents were purchased from Gibco (Waltham, MA, USA). Male beagle dogs at 10 months of age, body weight 13-15 kg, were provided by the Animal Laboratory of the Shanghai Sixth People's Hospital. The experimental protocol was reviewed and

approved by the hospital's Ethics Committee based on the Guidelines for the Ethical Treatment of Animals established by the International Council for Laboratory Animal Science (www.iclas.org).

Synthesis and characterization of USPIO

The synthesis of USPIO nanoparticles followed the protocols provided in our previous studies [20]. The detailed morphology of the synthesized Fe₃O₄ NPs was characterized using transmission electron microscopy (TEM) (JEM-2100F (JEOL, Japan)). The crystalline structure of the Fe₃O₄ NPs were monitored by an X-ray diffractometer (XRD, D8 ADVANCE, BRUKER-AXS) with Cu K α radiation ($\lambda = 0.15418$ nm) at a scan rate of 10 degrees per min and a 2θ scan range from 20° to 70°. Magnetization loop measurements were carried out with a Physical Property Measurement System (PPMS, Quantum Design, USA) EverCool-II with 9 Tesla magnets. The T2 relaxation times of the Fe₃O₄ NPs were obtained with a 1.4 T Bruker Minispec Analyzer (MQ60).

Cell culture

The primary culture of canine ADSCs and oral mucosal epithelial cells was prepared as reported previously [21]. Briefly, ADSCs were isolated by enzymatic digestion. After administering general anesthesia, researchers obtained primary ADSCs from fat tissue in the groin of beagle dogs and then digested the tissues with 0.1% collagenase I for 1 h at 37 °C. The primary ADSCs were maintained in low-glucose Dulbecco's modified Eagle's medium (DMEM) supplemented with 10% fetal bovine serum (FBS, Gibco). Primary oral mucosal epithelial cells were obtained from the buccal mucosa of beagle dogs. Small pieces of oral mucous membrane were excised from the bucca of the dogs. The harvested 1.5 cm \times 1.5 cm oral mucosa was washed 3 times with 0.25% chloramphenicol solution and digested overnight at 4 °C with 0.25% Dispase-II (protease from *Bacillus polymyxa*; Sigma). Then, the epithelial layer was separated with tweezers and digested in 0.05% pancreatic enzymes for 10 min; the rest of the submucosal connective tissue was cut into pieces and digested in 0.2% collagenase I for 2 h at 37 °C. The suspended cells were filtered, oral fibroblasts were cultured in high-glucose DMEM supplemented with 10% FBS, and oral mucosal epithelial cells were cultured in keratinocyte serum-free medium (K-SFM, Gibco) supplemented with epidermal growth factor and bovine pituitary extract. Primary cells at passage 1–2 were used in further experiments. The cell culture medium was changed at 1–2 day intervals.

Cell sheet preparation and identification

Oral mucosal epithelial cell sheet preparation and identification

The procedure for preparing oral mucosal epithelial cell sheets was based on published reports [22]. In brief, NIH 3T3 fibroblasts were cultured to 50%–60% confluence and incubated with 20 μ g mitomycin C per mL for 2 h at 37 °C, then washed twice with phosphate-buffered saline (PBS). 5 \times 10⁴ per cm² oral mucosal epithelial cells at passage 1 were co-cultured with mitomycin C-inactivated 3T3 fibroblasts. After co-culture *in vitro* for 10 days at 37 °C in a 5% CO₂–95% air incubator, epithelial cell sheets 20–25 μ m in thickness were obtained by reducing the temperature to 20 °C. The medium was replaced every 2 days. Hematoxylin and eosin (HE) staining and scanning electron microscopy (SEM) (SU8000 series; HITACHI, Tokyo, Japan) were used to observe the morphological features. Immunohistochemical staining for cytokeratin was used to prove the epithelial origin.

Oral fibroblast cell sheet preparation and identification

Fibroblasts at passage 2 were harvested for preparation of the cell sheet. To create cell sheets, fibroblasts at 1 \times 10⁵ per cm² were seeded in a 60-mm temperature-responsive cell culture surface (Thermo Fisher Scientific, San Jose, CA, USA). When the cells reached 90%–100% confluence, the fibroblasts were stimulated with 100 μ g/mL vitamin C (Sigma) for 21 days. The culture medium was composed of high-glucose DMEM, 10% FBS, 100 μ g/mL vitamin C, 3.7 g/L sodium bicarbonate (Sigma), 100 U/mL penicillin, and 100 mg/mL streptomycin sulfate. The culture medium was replaced every 2 days. After fibroblasts were cultured for 21 days at 37 °C in 5% CO₂, the culture temperature was reduced to 20 °C for 30 min to obtain intact fibroblast cell sheets. Likewise, HE staining and SEM were used to observe the morphological features. Immunohistochemical staining for vimentin was used to prove the fibrillar connective tissue origin.

Myoblast induction of ADSCs sheets: preparation and identification

Vigorous ADSCs were harvested for further experiments. To create cell sheets, ADSCs at 5 \times 10⁴ per cm² were seeded, and the myoblast differentiated culture medium was composed of low-glucose DMEM, 10% FBS, 5% horse serum (Gibco), 10 μ M 5-azacytidine (Sigma), 3.7 g/L sodium bicarbonate (Sigma), 100 U/mL penicillin, and 100 mg/mL streptomycin sulfate. At 90%–100% confluence, the

ADSCs were stimulated with 100 µg/mL vitamin C for 3 days, and then 50 µg/mL vitamin C for 18 days to form an ECM. Similarly, HE staining and SEM were used to observe the morphological features. Immunohistochemical staining for muscle protein markers, including desmin, α-SMA, and PAX7 was used to establish successful myoblast differentiation.

Scanning electron microscopy

The cell sheets sized 1.0 × 1.0 cm were washed with PBS 3 times and fixed with 2.5% glutaraldehyde in PBS for 2 h. After a thorough wash with PBS, the cells were dehydrated by a gradual change in the concentration of ethanol and then dried by lyophilization. The specimens were then sputter coated with platinum and examined by SEM.

Cell sheets labeled by USPIO

Polyamine poly-L-lysine (PLL) can effectively boost the intracellular uptake of nanoparticles via electrostatic interactions [23]. PLL hydrobromide (Sigma) was also used as the transfection agent in our experiments. Literature reports show that various concentrations of PLL have been used, ranging from 0.375 µg/mL to 1.5 µg/mL [12, 24, 25]. Excessive PLL can form toxic aggregates and inhibit the incorporation of nanosized iron oxide particles in the cells, so we chose a moderate concentration of PLL at 0.75 µg/mL. The seed cells were grown to 90% confluence. Epithelial cells were incubated with 25 µg Fe/mL USPIO and 0.75 µg/mL PLL. For ADSCs and fibroblasts, the incubation concentration of USPIO was 50 µg Fe/mL and 0.75 µg/mL PLL. The cell cultures were kept for 12 h at 37 °C in a 5% CO₂ atmosphere. After incubation for 12 h, cells were washed 3 times with PBS and were further cultured in the corresponding medium to form cell sheets.

Fabrication of a tissue-engineered bionic urethra

After cell sheet formation, we reduced the culture temperature to 20 °C for 30 min to detach the cell sheet from the 60-mm culture dish (Thermo Fisher Scientific). A medical-grade silicone tube was used as a template; the tube diameter was 4 mm and the tube length was 25 mm. According to the thickness of the 3 normal urethra layers (including, from the inside to the outside, the mucosa, submucosa, and muscularis), 2 harvested oral mucosal epithelial cell sheets were stacked together to form the epithelial layer, 1 harvested fibroblast cell sheet was used as the submucosal layer, and 2 myoblast differentiated ADSCs sheets were stacked together to form the muscular layer. The stacked cell sheets were in turn gently rolled into a tube around the silicone tube. The cell sheet layers stuck to each other to form a strong,

well connected structure. Then, USPIO-labeled and unlabeled tissue-engineered bionic urethras were transplanted subcutaneously into autologous groin tissue for 3 weeks to promote the revascularization and biomechanical strength of the implants. Meanwhile, as a comparison group, cell-free small intestinal submucosa (SIS) grafts (Cook Urological, Spencer, IN, USA) was also subcutaneously implanted into groin tissue.

Beagle dog urethroplasty with tissue-engineered bionic urethras

Three weeks after subcutaneous transplantation, SIS grafts, USPIO-labeled and unlabeled tissue-engineered bionic urethras were withdrawn and the medical-grade silicone tubes were removed. Twenty-four male beagle dogs were divided randomly into 4 groups of 6 each. Group 1 underwent tubularized substitution urethroplasty using USPIO-labeled tissue-engineered bionic urethras; group 2 received unlabeled tissue-engineered bionic urethras; group 3 received cell-free SIS as a negative control; and group 4 received autologous buccal mucosa as a positive control. The urethras were retrieved 3 months after implantation. For all surgeries, the canines received general anesthesia with pentobarbital. The penile urethras were accessed through the ventral midline, and a 2-cm long sample of tubular urethral tissue was completely removed. Then, the grafts for each group were positioned into the urethral defects, and tubular replacements were implanted using strainless end-to-end anastomosis using 5-0 Vicryl sutures (Ethicon, NJ, USA). A 10 F urethral catheter was placed, and the wound was closed in layers using a routine method. The catheter was left to provide bladder drainage for 14 days after the surgery, and intravenous penicillin G (2 g/day) was given for 3 days after the surgery to prevent infection.

MRI tracking *in vivo*

For *in vivo* monitoring of the tissue-engineered bionic urethras labeled with USPIO and to facilitate understanding of the conditions of the labeled graft in the transplanted areas, the urethras of each group were examined by MRI at 3 months after transplantation. During the MRI, the animals were anesthetized with pentobarbital sodium (30 mg/kg IV). After use of a gradient-echo localizer in 3 spatial directions, the T2-weighted MRI scans were acquired using the Rapid Acquisition with Relaxation Enhancement sequence, based on specific parameters as follows: TE = 71 ms, TR = 3500 ms, RARE factor = 8, number of averages = 8, slice thickness = 1 mm, FoV = 70 × 100 mm, and matrix = 384 × 384.

Postoperative evaluation

Retrograde urethrograms were performed at 3 months postoperatively. After the retrograde urethrograms, 6 animals in each group were humanely euthanized, and the appearance of each alternative urethra was evaluated by visual inspection.

Histological analysis

Hematoxylin and Eosin staining

The oral mucosal epithelial cell sheet, the oral fibroblast cell sheet, the myoblast induction of ADSCs sheet, SIS, autologous buccal mucosa and the tissue-engineered bionic urethras were fixed in 4% paraformaldehyde for 12 h and embedded in paraffin. Then, 5 mm serial sections were generated and evaluated by HE staining. Furthermore, the urethras for each group were harvested at 3 months postoperatively and stained with HE.

Prussian blue staining

The intracellular iron oxide distribution was detected using a Perls' Prussian blue staining kit (Beijing Solarbio Science & Technology, Beijing, China). The sections were fixed for 15 min in 4% paraformaldehyde and then incubated for 25–30 min with 10% potassium ferrocyanide, rewashed twice with PBS, and counterstained with Nuclear Fast Red for 10 min. Cells containing intracytoplasmic blue granules were defined to be Prussian blue (PB) staining-positive (PB-positive).

Immunohistochemistry

Immunohistochemical analysis was performed using anti- α -SMA (1:1500 dilution, Sigma), PAX7 (1:800 dilution, Sigma), and desmin (1:500 dilution, Santa Cruz Biotech, Santa Cruz, CA, USA) to observe the expression of myoblast-differentiated protein in myoblast induction of ADSCs sheets; anti-pan cytokeratin antibody (AE1 + AE3) (1:500 dilution, Abcam) and anti-vimentin antibody (1:300 dilution, Santa Cruz Biotech) were used to verify the epithelial origin and fibrillar connective tissue origin, respectively. Sections were heated in 10 mM Tris-HCl buffer (pH 8.8) containing 1 mM EDTA using an autoclave for antigen retrieval and then blocked in Tris-buffered saline containing 5% bovine serum albumin and 0.1% Tween 20 for 1 h at room temperature. The samples treated with the primary antibodies were incubated overnight at 4°C, followed by washing 5 times with PBS. The sections were then incubated for 1 h at room temperature in an appropriate secondary antibody, followed by subsequent linking to horseradish peroxidase and substrate/chromogen reaction using an

immunoperoxidase secondary detection kit (Millipore, Billerica, MA, USA). Negative controls without primary antibodies were also prepared to rule out nonspecific labeling.

Immunofluorescence

The tissue-engineered bionic urethras and retrieved urethras for each group at 3 months were fixed in 4% paraformaldehyde for 12 h and were embedded in paraffin. Sections were then permeabilized with 0.2% Triton X-100 (Invitrogen) and blocked with 5% bovine serum albumin for 30 min. Then, to observe the vascular expression, sections were incubated with an optimal concentration of rabbit monoclonal anti-CD34 antibody (1:150, Abcam) overnight at 4 °C, then incubated with anti-rabbit secondary antibody (1:500; Alexa Fluor 470; Invitrogen) for 45 min at 37 °C, followed by washing 3 times with PBS. The cell nucleus was stained with 4'-6-diamidino-2-phenylindole (DAPI, 1:1000, Vendor Name, City, Country) for 30 s. To observe the layered structure of the tissue-engineered bionic urethras and retrieved urethras, sections were incubated with an optimal concentration of rabbit polyclonal anti-Desmin antibody (1:500 dilution, Santa Cruz Biotech), mouse monoclonal anti-pan Cytokeratin antibody [AE1+AE3] (1:300, Abcam) overnight at 4 °C, then incubated with anti-rabbit Alexa Fluor 560 secondary antibody (1:500, Invitrogen) and anti-mouse Alexa Fluor 470 secondary antibody (1:500, Invitrogen), followed by rinsing 3 times with PBS. Nuclei were counterstained with DAPI (1:1000, Invitrogen). The vascular expression and hierarchical structure of the urethras were observed under an Axiovert 200 fluorescence microscope (Carl Zeiss Inc., Thornwood, NY, USA).

Statistical analysis

Data were expressed as means \pm standard deviations. SPSS 17.0 (IBM, Armonk, NY, USA) was used for statistical analysis. The *t* test, the chi-square test, and one-way analysis of variance (ANOVA) were used to determine the statistical significance of blood vessel density and postoperative evaluation among groups, and a value of $P < 0.05$ was considered statistically significant.

Results

Characterization of USPIO

Representative TEM images showed the synthesized USPIO has a spherical appearance, uniform size with a diameter of about 7.217 ± 1.176 nm (Fig.1a-b), close to the calculated diameter of 7.57 nm from the strongest peak (311) observed in XRD

(Figure 1c). Figure 1c also shows that the XRD pattern of the synthesized nanoparticles is in good agreement with that of the standard cubic phase structure [26]. And then, the value of T2 relaxation rate Fe₃O₄ NPs was 264.6 mM⁻¹ s⁻¹ (Fig.1d), which was better than other results reported in literature [27]. These results indicate that the prepared USPIO are ideal for use as contrast agent for clinical diagnosis.

Cell sheet formation and identification

Oral mucosal epithelial cell sheets, oral fibroblast cell sheets, and myoblast induction of ADSCs sheets were obtained by the reduced temperature method at 20°C for 30 min. Cell sheets exhibited the typical cross-linking structures with cells and abundant ECM (Fig.2A). The HE staining showed the mean thicknesses of the oral mucosal epithelial cell sheets, the oral fibroblast cell sheets, and the myoblast induction of ADSCs sheet were about 25 μm, 60 μm, and 90 μm, respectively (Fig.2A). SEM images of oral mucosal epithelial cell sheets showed the characteristic cobblestone morphology; oral fibroblast cell sheets displayed an even and flattened distribution with abundant fiber cords; and myoblast induction of ADSCs sheets revealed tight cell junctions and aligned in a striated pattern and fused into a myotube-like fiber (Fig.2A). Immunohistochemistry results showed positive staining of vimentin and pan cytokeratin (AE1+AE3) in oral fibroblast cell sheets and oral mucosal

epithelial cell sheets, which respectively verify the fibrillar connective tissue origin and the epithelial origin (Fig.2B). Furthermore, after 3 weeks of culture with myoblast differentiation medium, the myoblast induction of ADSCs sheets showed positive expressions of α-SMA, desmin, and PAX7, which were used as markers of muscle cell differentiation (Fig.2B).

Fabrication of a tissue-engineered bionic urethra

In macroscopic examinations, the cell sheet was a white membrane that had sufficient mechanical stability to be handled by forceps. A tissue-engineered bionic urethra was created by an orderly wrapping various cell sheets around silicone tube. The tube was first wrapped with 2 layer oral mucosal epithelial cell sheets, then 1 layer oral fibroblast cell sheet, and finally 2 layer myoblast induction of ADSCs sheets to create the bionic urethra. Due to the abundant ECM distribution in the cell sheets, the cell sheets stuck together and did not easily fall apart. The cell sheets were tubularized to form a tissue-engineered bionic urethra 2.5 cm long and 4mm in diameter. After subcutaneous transplantation for 3 weeks, the constructs maintained a good cylindrical shape with adherent subcutaneous tissue. Cell-free SIS and the autologous buccal mucosa were used as control groups in our experiment (Fig.3).

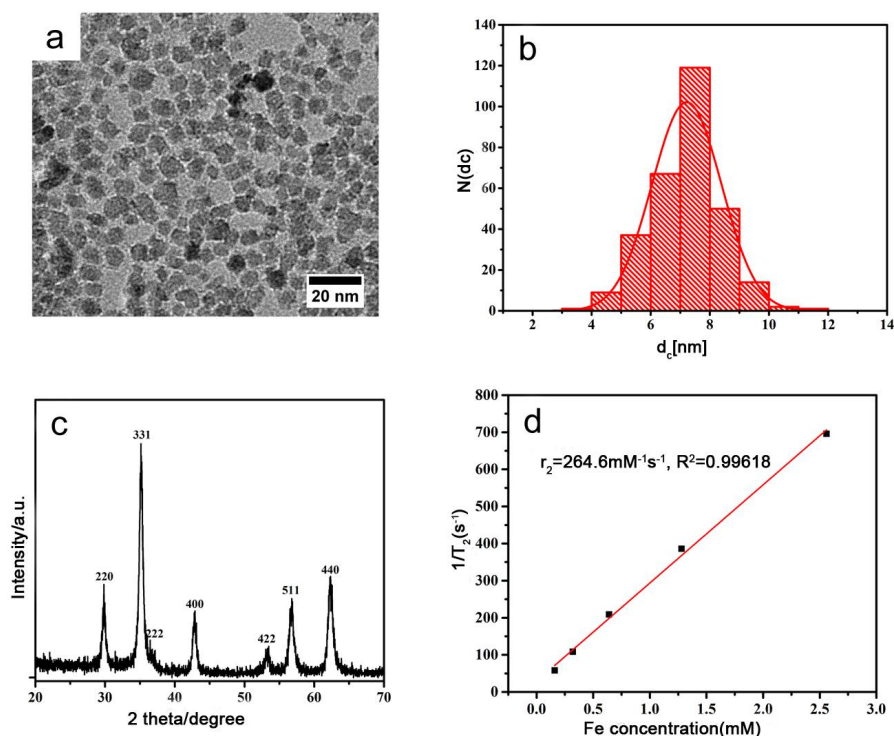


Figure 1. Characterization of USPIO (a) TEM image; (b) the diameter distribution from TEM; (c) The XRD pattern of the synthesized USPIO; (d) The value of T2 relaxation rate of the synthesized USPIO as a function of Fe concentration from MRI of USPIO in tissue-engineered bionic urethra.

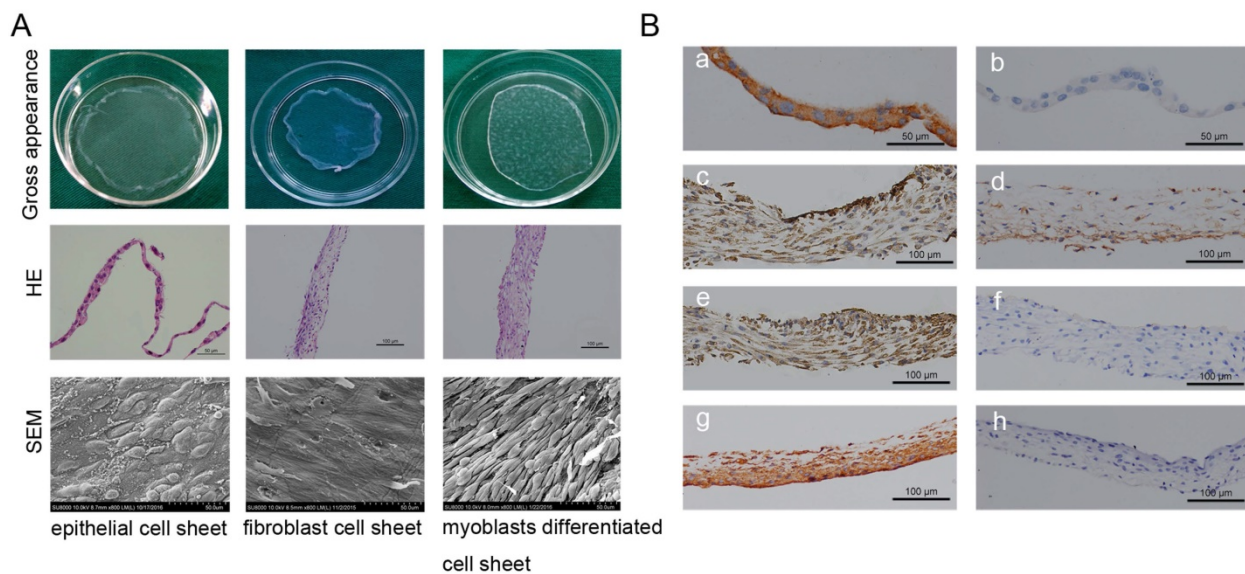


Figure 2. Cell sheet formation and identification. (A) Cell sheet formation after 21 days of continuous culture. The first line shows photographs of each of the types of cell sheets; the second line show HE staining results of three cell sheets, which revealed that the cultured oral mucosal epithelial cell sheets were composed of 2–3 layers of cells (left, scale bar: 50µm), the cultured oral fibroblast cell sheets were composed of 3–4 layers of cells (middle, scale bar: 100µm), and the cultured myoblast induction of ADSCs sheets were composed of 6–7 layers of cells(right, scale bar: 100µm); the third line shows the SEM images of the three cell sheets, scale bar: 50 µm. (B) Immunohistochemical identification of three types of cell sheets. The result of immunohistochemistry revealed, positive staining of pan cytokeratin (AE1+AE3) in oral mucosal epithelial cell sheets (a), b is the negative control; positive expressions of muscle protein markers in myoblast induction of ADSCs sheets after 3 weeks of culture with myoblast differentiation medium, including α-SMA (c), PAX7 (d) and Desmin (e), f is the negative control; positive staining of vimentin in oral fibroblast cell sheets (g), h is the negative control. Scale bar: 100 µm.

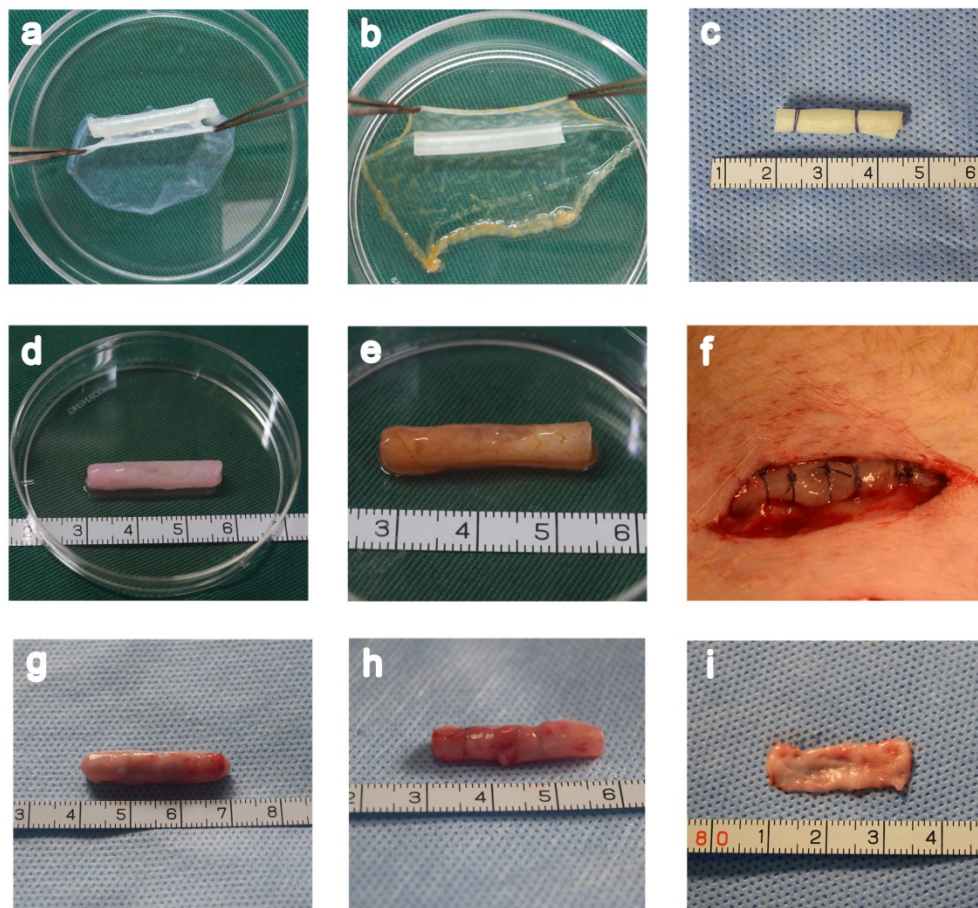


Figure 3. Fabrication of a tissue-engineered bionic urethra. A unlabeled and USPIO-labeled tissue-engineered bionic urethra were fabricated by wrapping a silicone tube with a stack of three types of cell sheets in a carefully planned order (a and b). As a control, cell-free SIS was also wrapped around the silicone tube (c) and transplanted to subcutaneous area. The length of bionic urethra is 2.5 cm and its diameter is 4 mm (d). The yellowish-brown in USPIO-labeled tissue-engineered bionic urethra is due to the characteristic color of iron nanoparticles (e). The bionic urethra was auto-transplanted into subcutaneous space of groin for 3 weeks (f). Three weeks after subcutaneous transplantation, for tissue-engineered bionic urethra (g) and cell-free SIS (h), the retrieved implant maintained a good cylindrical shape and mechanical strength better than prior to transplantation due to the growth of tissue around the implant. The autologous buccal mucosa is the material commonly used for urethra reconstruction in the clinical setting, the size is 2.5 cm×1.0 cm (i).

Urethral reconstruction after transplantation of tissue-engineered bionic urethras

Tubularized penile urethral replacement was performed with the retrieved implants and autologous buccal mucosa. At 3 months after full-thickness urethral reconstruction, retrograde urethrograms were used for the urethral assessment, including urinary ulcerations, strictures, diverticula, and fistulas. All dogs in the experiment were humanely killed after this assessment. The result of retrograde urethrograms indicated, similar to normal urethra, the 6 dogs in either group 2 (bionic urethra implants) and 4 (buccal mucosa implants) voided fluently without major urinary complications. In contrast, severe urethra strictures (4 dogs) or urinary fistulas (2 dogs) were found in group 3 (SIS implants) ($P < 0.05$) (Fig.4A). Macroscopic examination of the retrieved urethras confirmed the absence of ulcerations, strictures, and fistulas in groups 2 and 4, but extensive scarring and contracture tissue at the graft site was found in group 3. At 3 months post-transplantation, the junction between the native urethra and the grafts of groups 2 and 4 were indiscernible to the naked eye. (Fig.4B). Prior to implanting, histologic analysis showed that when the constructs were first made the wall of the bionic urethra was composed of multilayer cell sheets and there was a certain gap among cell sheets observable using microscopy (magnification $200 \times$). After subcutaneous transplantation for 3 weeks, the cell sheets got closer together and 3 months after surgery demonstrated that, similar to normal urethra, multilayered tissue were observed in bionic urethra transplantation (group 2). Three weeks after subcutaneous implantation, the cell-free SIS maintained its structure and morphology, and cells infiltration was observed at the edge of transplanted SIS. In group 3 with cell-free SIS for urethral replacement, after 3 months urethra transplantation, the SIS was not observed at the transplant site. Additionally, tissue structures were not clear and there was a lack of epithelial cell coverage coupled with obvious fibrosis formation indicating a lack of urethral repair. In group 4 with autologous buccal mucosa for urethral replacement, stratified epithelia covered the graft site with no strictures (Fig.4C).

USPIO labeling and MRI tracking *in vivo*

Based on findings reported in previous literature reports, we chose a moderate concentration of USPIO labeling at $25 \mu\text{g Fe/mL}$ for epithelial cells and $50 \mu\text{g Fe/mL}$ for ADSCs and fibroblasts all of which showed a labeling efficiency of nearly 100%. This

concentration did not impair cell survival, self-renewal, or proliferation capacity (data not shown). Prussian blue staining revealed blue-stained granules (iron particles) exclusively distributed in cell sheets (Fig. 5A). Due to shortening of $T2^*$ and $T2$ relaxation times measured via MRI, the USPIO is observed as hypointensity on $T2^*$ -weighted and $T2$ -weighted images. In our study, USPIO-labeled tissue-engineered bionic urethra (group 1) can be effectively visualized by MRI, manifesting as hypointense regions on $T2$ images in the transplantation sites of the anterior urethra, while transplanted with unlabeled tissue-engineered bionic urethra (group 2) and normal urethra at 3 months after transplantation showed no cell signal (Fig.5B). Prussian blue staining showed the blue-stained iron particles were abundant in retrieved urethras and the result was consistent with the MRI images (Fig.5A).

Vascularization in unlabelled tissue-engineered bionic urethras

The number of the newly formed vessels was quantified following the initial establishment of the constructs, after 3 weeks subcutaneous transplantation, and finally 3 months after urethral reconstruction. The small vessel endothelium was stained with a marker of CD34. Five nonconsecutive tissue sections were randomly selected from each group. Measurement and quantification were performed within the $10 \text{ random} \times 200$ magnification fields, and the average number of vessels per field are expressed as the density of vessels. The results of immunofluorescence analysis showed almost no blood vessels when the constructs were initially implanted, but at 3 weeks after subcutaneous transplantation, the density of vessels was significantly increased and formed a new network of blood vessels. After *in vivo* transplantation, the density of vessels was further up-regulated ($P < 0.05$) and approached the density of normal urethral tissue ($P > 0.05$) (Fig.6).

Immunofluorescence analysis of urethral hierarchy

Immunofluorescence analysis (Fig.7) further revealed that the urethral grafts of groups 1 and 2 maintained their 3-layer construction, including epithelial cells labeled with green fluorescence (epithelial layer) and muscle cells labeled with red fluorescence (muscular layer). The thickness of epithelial layer did get thicker after transplantation *in vivo* and ensured the continuity and closeness of the urinary tract lumen.

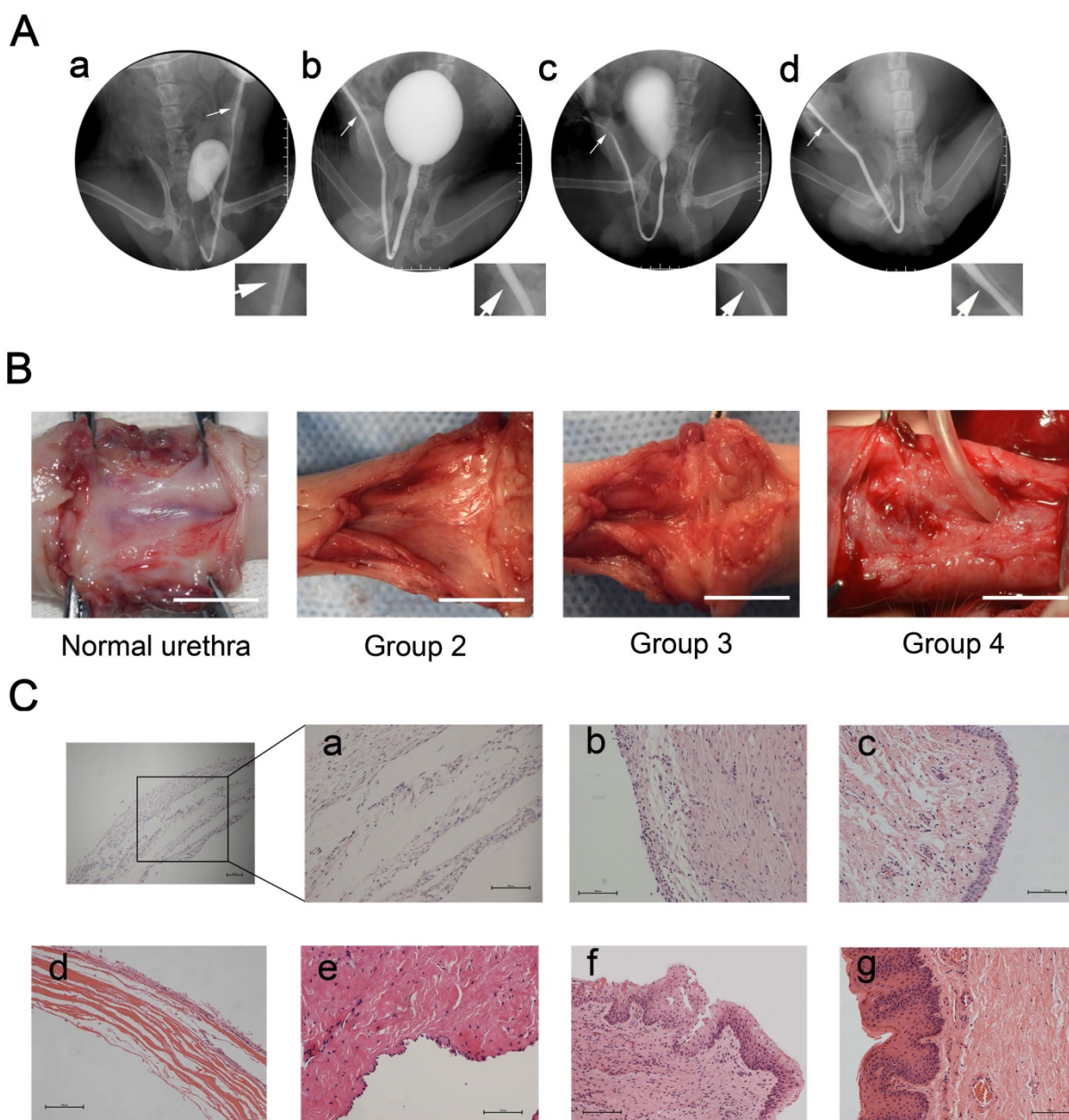


Figure 4. Urethral reconstruction after transplantation of tissue-engineered bionic urethras. (A) After 3 months transplantation, similar to normal urethra (a), the retrograde urethrography in group 2 with bionic urethra transplantation (b) and group 4 with autologous buccal mucosa transplantation (d) indicated the maintenance of a wide urethral caliber without stricture. In the group 3 with SIS grafts (c), the urethrography showed urethra strictures of varying degrees. (B) Macroscopic examination of retrieved urethra at 3 months after full-thickness urethral reconstruction. Similar to normal urethra, no ulcerations, strictures, and fistulas were observed in groups 2 (bionic urethra implants) and 4 (buccal mucosa implants), but extensive contracture and scarring tissue at the graft site was found in group 3 (SIS grafts). scale bar: 1.0 cm. (C) Histologic analysis results. a): the initial establishment of the constructs, b): subcutaneous transplantation of bionic urethra for 3 weeks, c): 3 months after urethra replacement in group 2 (bionic urethra implants), d): subcutaneous transplantation of cell-free SIS for 3 weeks, e): 3 months after urethra replacement in group 3 (SIS grafts), f): 3 months after urethra replacement in group 4 (buccal mucosa implants), g): normal urethra. scale bar: 100 μ m.

Discussion

In clinical practice, urinary tract diseases are often associated with full-thickness urethral defects, including the epithelial layer, the fibrous layer, and the muscular layer. Thus, the ideal material for urethral repair and replacement must act as a frame for the growth of host urethral wall components and finally become an integrated part of the urethral wall

with the same mechanical and functional properties as those of the host. In this study, we established tissue-engineered bionic urethras with similar physical structures using cell sheet technology and tracked the constructs by USPIO, and furthermore proved the feasibility of the constructs for full-thickness urethral reconstruction, and the scheme diagram is shown in Fig.8.

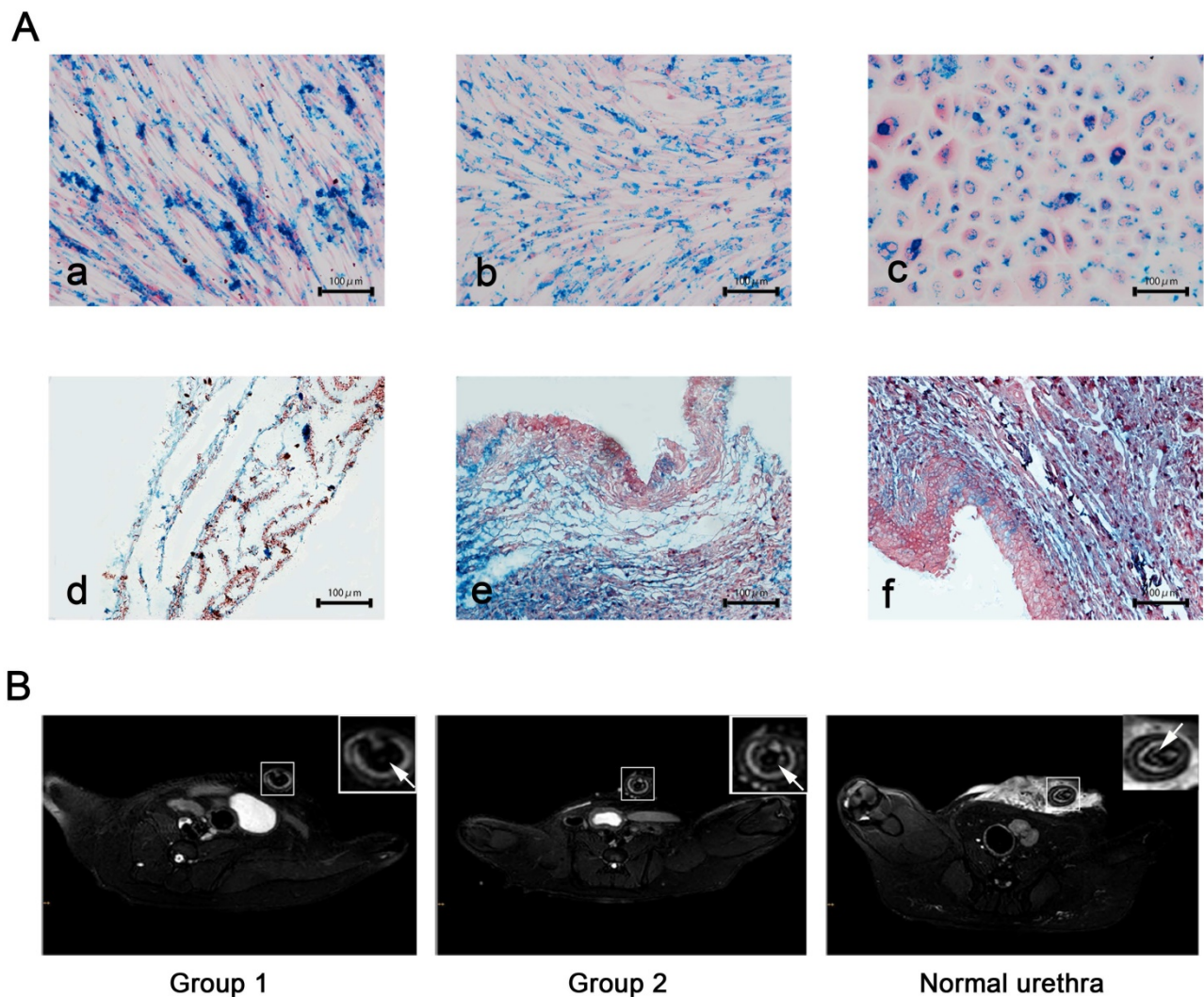


Figure 5. USPIO labeling and MRI tracking *in vivo* (A) Prussian blue staining for iron content and labeling efficiency. a): USPIO-labeled myoblast induction of ADSCs sheets, b): USPIO-labeled oral fibroblast cell sheets, c): USPIO-labeled oral mucosal epithelial cell sheets, d): the initial establishment of the USPIO-labeled constructs, e): subcutaneous transplantation for 3 weeks, f): USPIO-labeled bionic urethra transplantation in group 1. Scale bar: 100 μ m. (B) After 3 months of urethral replacement, MRI detection of the transplanted tissue-engineered bionic urethra *in vivo*. The urethra wall was detected on T2-weighted images, the MRI signal intensity of unlabeled bionic urethra (group 2) was similar to normal urethra, presenting as gray-white distribution. However, because of the existence of USPIO, the urethra wall of USPIO-labeled bionic urethra (group 1) was behaved for low signal intensity and black signal area, arrowheads toward the wall of urethra. Scale bar: 1.0 cm.

Urethral strictures or defects may be repaired by various types of tissue engineering technology, including acellular scaffolds or seeding cells onto either decellularized or biodegradable scaffolds. For acellular scaffolds, the maximum defect distance suitable for tissue regeneration appears to be only 0.5 cm [28]. Seeding various types of cells onto biodegradable scaffolds for urethral repair has been proven to be more effective than using only acellular scaffolds in previous studies, including acellular collagen matrix [29, 30], bladder acellular matrix [31-33], silk fibroin matrices [34], SIS [35], and acellular corpus spongiosum matrix [36]. However, the cell-scaffold complex also has many shortcomings. First, attached cells must be separated into cell suspensions by trypsin digestion before cell seeding,

which may affect the cell activity, destroy the ECM and cell-cell junctions. Next, some cells cannot adhere well onto scaffolds and the depth of infiltration is inconsistent, which leads to cell loss and causes uneven cell distribution. Furthermore, graft materials could trigger the body's immune response, including humoral and cellular immunity. Finally, scaffold materials have different degradation speeds that may influence the integrity and smoothness of the urethral surface.

Cell sheet technology can effectively solve these problems. Cell sheets are fabricated by the combination of ECM and autologous cells without biomaterial scaffolds and trypsin digestion, bypass immunologic reactions, and provide native ECM and a specific cellular microenvironment for tissue

regeneration. Furthermore, abundant growth factors were found in ECM. Hodde *et al.* [37] showed each gram of ECM contains as much as 0.77 ng of vascular endothelial growth factor that promotes cell growth and angiogenesis. Previously, Mikami *et al.* [38] fabricated two-layer tissue-engineered urethra grafts by combining autologous oral epithelial cell sheets with collagen mesh matrices seeded with muscle cells that were grafted to cover a 2-cm urethral defect in a canine model and promoted the regeneration of a functional urethra. However, the 2-layer urethra without a fibrous layer is a loose construction that may lack adequate mechanical strength and revascularization for the submucosal layer of urethral vessels could not be regenerated. Due to their release of cytokines, growth factors, and collagen, fibroblasts can effectively improve the mechanical properties of the grafts via keratinocyte expansion [39]. Compared with skin fibroblasts, oral mucosal fibroblasts exhibit increased levels of active matrix metalloproteinase 2 and decreased levels of tissue inhibitors of metalloproteinases that increase extracellular matrix reorganizational ability and reduce scar formation

[40]. The presence of oral fibroblast cell sheets in the bionic urethra could reduce or prevent scarring and contraction after grafting. In addition, cell sheets require a great quantity of seed cells, but the proliferative ability of myoblasts is relatively weak and the raw materials for autologous myoblasts are limited, thus it is difficult to provide sufficient myoblasts to establish a tissue-engineered bionic urethra. Compared to other types of mesenchymal stem cells, ADSCs possess the highest proliferation potential and exhibit high tolerance to serum deprivation-induced apoptosis [41]. Moreover, ADSCs can be successfully induced to differentiate into myoblasts by 5-azacytidine and have been reported to treat muscle disorders by our group and others [19, 42, 43]. In our experiments, we took autologous ADSCs as seed cells, promoted their muscle differentiation with 10 μ M 5-azacytidine and 5% horse serum, and built the muscular layer of bionic urethras. Thus, we chose ADSCs, oral epithelial cells and oral fibroblasts as seeding cells to form cell sheets and build a real bionic urethra with a 3-layer structure.

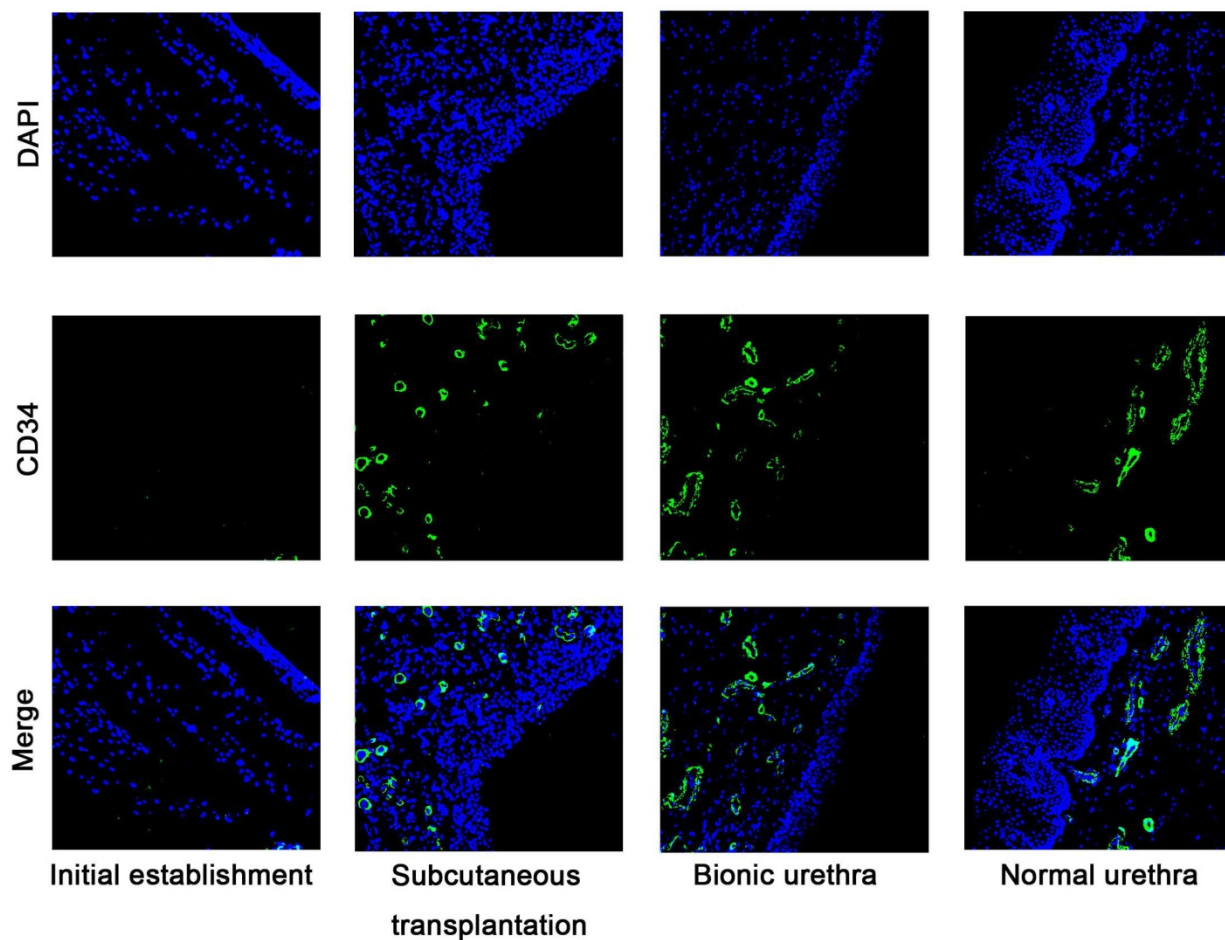


Figure 6. Immunofluorescence staining images of CD34 at pre- and post-transplantation. Almost no blood vessels were observed when the constructs were initially established, but after 3 weeks of subcutaneous transplantation, the density of vessels was significantly increased. After 3 months *in vivo* transplantation, the density of vessels was further up-regulated ($P < 0.05$) and approached the density of normal urethral tissue ($P > 0.05$). scale bar: 100 μ m.

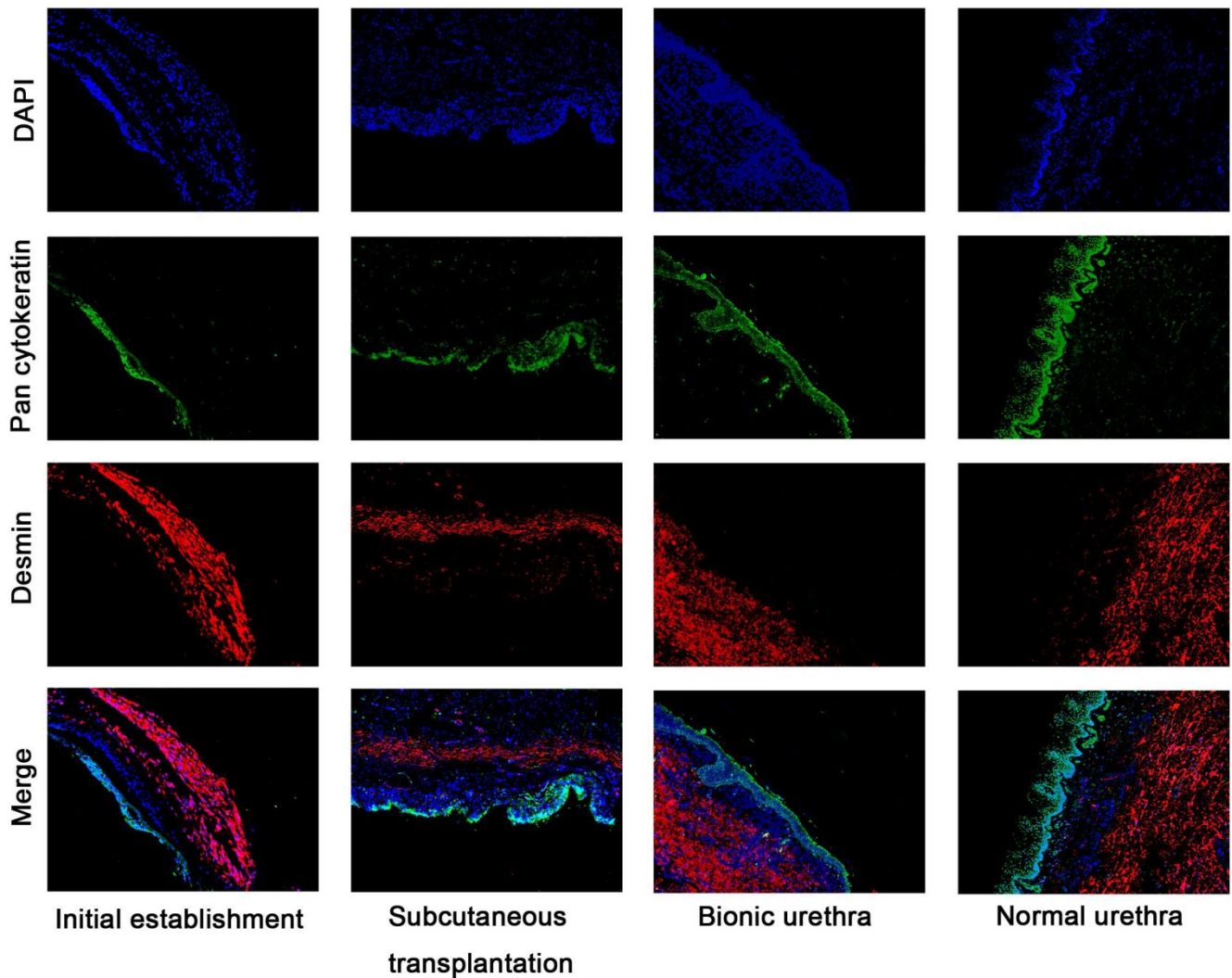


Figure 7. Immunofluorescence analysis of hierarchical structure of the urethras. Fluorescence microscopy reveals epithelial cells labeled with green fluorescence (Pan cytokeratin AE1+AE3) and myoblast labeled with red fluorescence (Desmin), DAPI staining identifies all cell nuclei (blue), scale bar: 100µm.

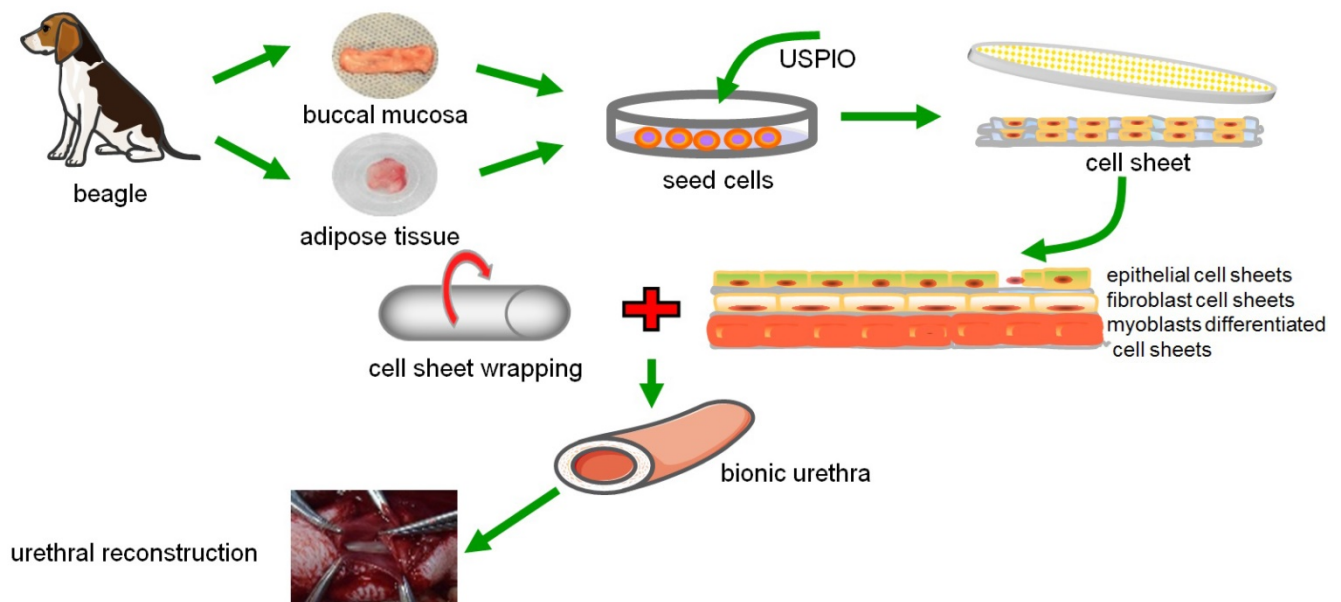


Figure 8. The scheme diagram of tissue-engineered bionic urethras using cell sheet technology.

The submucosal layer of the urethra contains abundant capillaries to supply nutrients and oxygen to urethral tissue. Thickened soft tissue cannot be fabricated by simple repeated stacking of cell sheets, mainly because the formation of vascular networks is insufficient to supply oxygen and nutrients for the thickened tissue, which often leads to epithelial cell necrosis and shedding. Thus, promoting the formation of new blood vessels is a key point *in vivo*. Graft revascularization can be promoted by subcutaneous transplantation. Shimizu *et al.* [44] showed that repeated subcutaneous transplantation of triple-layer grafts can lead to the fabrication of 1-mm-thick, functional, cell-dense cardiac tissue grafts (30-layer cell sheets) with well-organized microvascular networks. CD34 is a unique surface antigen expressed in endothelial cell at sites of active angiogenesis *in vivo* [45], and thus we chose immunofluorescence for CD34 to monitor revascularization during the initial establishment of constructs, subcutaneous transplantation at 3 weeks, and at 3 months after urethral reconstruction. Experimental results showed the number of new blood capillaries in tissue-engineered bionic urethras significantly increased after subcutaneous transplantation, and the construct possessed an intact epithelial layer without exfoliation of epithelial cells. Although the blood capillaries had not totally reached the levels of normal urethras, vascular density and arterial diameter were found to be further increased after 3 months of full-thickness urethra replacement *in vivo*. Structurally, the bionic urethra had a clear structural hierarchy and was covered by several layers of epithelial cells, which indicates that the new blood vessels provide sufficient nutrition and oxygen to ensure the cells survive and maintain the urinary tract functions. Subcutaneous transplantation is feasible to promote graft angiogenesis, and the new blood capillary network could connect with the host vasculature after ectopic replantation [46-48].

To assess the survival of transplanted USPIO-labeled bionic urethras after full-thickness urethral replacement, we further examined localized USPIO labeling using MRI in the transplanted area of the urethra over 3 months. In previous reports, several studies have suggested that the use of iron oxide nanoparticles for cell labeling is an effective MRI contrast for long-term detection of grafted cells and tissues in animal experiments. Neri *et al.* [49] proved that 5×10^3 to 1×10^4 viable USPIO-labeled human neural precursor cells could be detected after transplantation in the adult murine brain and could be tracked for at least 1 month in longitudinal studies. Moreover, Guzman *et al.* [50] detected the targeted migration and distribution of USPIO-labeled clusters

of cells up to 18 weeks. In our study, the tissue-engineered bionic urethra remained visible up to 3 months *in vivo* and presented a hypointense signal in the transplanted area of the anterior urethra on T2 images, which was further confirmed by PB staining on corresponding tissue. Moreover, the hypointense regions detected by MRI were closely associated with the amount of USPIO-labeled transplanted cells, and these results prove that cell survival remains stable for at least 3 months.

In general, the urethral stricture model was built using ligation, thermocoagulation, or urethrotomy in large animals [51]. Furthermore, some chemicals have been reported to have the ability to induce urethral fibrosis in animal models, such as transforming growth factor-beta 1 [52] and mitomycin C [53]. However, such urethral injuries may be superficial and offer a relatively good prognosis, but clinical instances of urethral stricture are generally associated with full-thickness urethra defects and are hard to repair. In our experiments, full-thickness urethra tissue was completely exfoliated from the urethral plate and was subsequently repaired with three different biological materials, including cell-free SIS, buccal mucosa and the bionic urethra. Unlike cell sheets that contain cells and ECM, SIS is composed only of ECM proteins and is derived from the small intestinal mucosa tissue of the pig. In previous studies, SIS appeared to be an effective and safe reconstructive material in the treatment of bulbar and penile urethral strictures [54, 55]. Furthermore, buccal mucosa graft urethroplasty is preferred to treat anterior urethral strictures and good therapeutic effects have been reported [56, 57]. Thus, we used cell-free SIS and buccal mucosa (with autologous cell) as the control groups for urethral replacement. Three months after urethroplasty, the cell-free SIS (group 3) was absorbed completely without obvious residual tissues and all the dogs in the group had urethral narrowing or urinary fistulas, which confirmed that ECM alone without cell construct is not suitable for full-thickness urethral reconstruction. For bionic urethra (group 2), histological examination indicated that a wide urethral caliber was maintained with no signs of stricture. Immunofluorescence results also showed the urethral hierarchy was restored, which showed the therapeutic efficacy is similar to group 4 (buccal mucosa graft) with potential therapy in clinical application.

However, this study has a few limitations. The major disadvantage lies in the long development cycles and complicated procedures required to fabricate tissue-engineered bionic urethras using cell sheet technology. Furthermore, long-term results of follow-up and long-segment urethral reconstruction

(>2cm) requires further evaluation in the follow-up study.

Conclusions

In this study, we demonstrated that tissue-engineered bionic urethras can be successfully constructed using stacked cell sheets of endothelial cells, fibroblasts, and myoblast induction of ADSCs, and the construct can be traced *in vivo* by MRI. Tissue-engineered bionic urethras were transplanted subcutaneously into the autologous groin for 3 weeks and promoted the revascularization of implants. The 3-layer epithelial-fiber-muscular tissue-engineered urethras can be successfully used in 2-cm full-thickness anterior urethral replacement, leading to improved outcomes of urethra-repair procedures, which provides a new choice for urethral reconstruction.

Acknowledgments

This project was supported by the National Natural Science Foundation of China (Grant Nos. 81270780, 81470917 and 81671737), the Doctorate Innovation Fund of Shanghai Jiao Tong University School of Medicine (Grant No. BXJ201636) and Leaders Training Program of Shanghai. The authors also acknowledge the technical assistance from the Professor Weixin Zhao and Professor Anthony Atala of the Wake Forest Institute for Regenerative Medicine, Winston Salem, NC, USA.

Competing Interests

The authors have declared that no competing interest exists.

References

- Summerton D-J, Kitrey N-D, Lumen N, Serafetinidis E, Djakovic N.EAU Guidelines on Iatrogenic Trauma. *Eur Urol.* 2012;62:628-39.
- Hampson L-A, McAninch J-W, Breyer B-N. Male urethral strictures and their management. *Nat Rev Urol.* 2013;11:43-50.
- Osman N-I, Patterson J-M, MacNeil S, Chapple C-R. Long-term follow-up after tissue-engineered buccal mucosa urethroplasty. *Eur Urol.* 2014;66:790-1.
- Barbagli G, Vallasciani S, Romano G, Fabbri F, Guazzoni G, Lazzeri M. Morbidity of oral mucosa graft harvesting from a single cheek. *Eur Urol.* 2010;58:33-41.
- Fu Q, Cao Y-L. Use of tissue engineering in treatment of the male genitourinary tract abnormalities. *J Sex Med.* 2010;7:1741-6.
- Sievert K-D, Amend B, Stenzl A. Tissue engineering for the lower urinary tract: a review of a state of the art approach. *Eur Urol.* 2007;52:1580-9.
- Takeuchi R, Kuruma Y, Sekine H, Dobashi I, Yamato M, Umezumi M, et al. In vivo vascularization of cell sheets provided better long-term tissue survival than injection of cell suspension. *J Tissue Eng Regen Med.* 2014.
- Sasagawa T, Shimizu T, Sekiya S, Haraguchi Y, Yamato M, Sawa Y, et al. Design of prevascularized three-dimensional cell-dense tissues using a cell sheet stacking manipulation technology. *Biomaterials.* 2010;31:1646-54.
- Yang J, Yamato M, Kohno C, Nishimoto A, Sekine H, Fukai F, et al. Cell sheet engineering: recreating tissues without biodegradable scaffolds. *Biomaterials.* 2005;26:6415-22.
- Cerqueira M-T, Pirraco R-P, Martins A-R, Santos T-C, Reis R-L, Marques A-P. Cell sheet technology-driven re-epithelialization and neovascularization of skin wounds. *Acta Biomater.* 2014;10:3145-55.
- Elias A, Tsourkas A. Imaging circulating cells and lymphoid tissues with iron oxide nanoparticles. *Hematology Am Soc Hematol Educ Program.* 2009:720-6.
- Mishra S-K, Khushu S, Gangenahalli G. Potential stem cell labeling ability of poly-L-lysine complexed to ultrasmall iron oxide contrast agent: An optimization and relaxometry study. *Exp Cell Res.* 2015;339:427-36.
- Xu C, Miranda-Nieves D, Ankrum J-A, Matthies M-E, Phillips J-A, Roes I, et al. Tracking Mesenchymal Stem Cells with Iron Oxide Nanoparticle Loaded Poly(lactide-co-glycolide) Microparticles. *Nano Lett.* 2012;12:4131-9.
- Chen R, Yu H, Jia Z-Y, Yao Q-L, Teng G-J. Efficient nano iron particle-labeling and noninvasive MR imaging of mouse bone marrow-derived endothelial progenitor cells. *Int J Nanomedicine.* 2011;6:511-9.
- Oude-Engberink R, Van-Der-Pol S, et al. Comparison of SPIO and USPIO for in vitro labeling of human monocytes: MR detection and cell function. *Radiology.* 2007;243:467-74.
- Mertens ME, Hermann A, Bühren A, Olde-Damink L, Möckel D, Gremse F, et al. Iron Oxide-labeled Collagen Scaffolds for Non-invasive MR Imaging in Tissue Engineering. *Adv Funct Mater.* 2014;24:754-62.
- Zhou S, Yin T, Zou Q, Zhang K, Gao G, Shapter J-G, et al. Labeling adipose derived stem cell sheet by ultrasmall super-paramagnetic Fe₃O₄ nanoparticles and magnetic resonance tracking in vivo. *Sci Rep.* 2017;7:42793.
- Lu M, Zhou G, Liu W, Wang Z, Zhu Y, Yu B, et al. Remodeling of buccal mucosa by bladder microenvironment. *Urology.* 2010;75:1514 e7-14.
- Fu Q, Song X-F, Liao G-L, Deng C-L, Cui L. Myoblasts Differentiated From Adipose-derived Stem Cells to Treat Stress Urinary Incontinence. *Urology.* 2010;75:718-23.
- Gao G, Zhang Q, Cheng X-B, Shapter J-G, Yin T, Sun R, et al. Ultrafine ferromagnetic nanoparticles embedded into mesoporous carbon nanotubes for lithium ion batteries. *Sci Rep.* 2015;5:17553.
- Fu Q, Deng C-L, Zhao R-Y, Wang Y, Cao Y. The effect of mechanical extension stimulation combined with epithelial cell sorting on outcomes of implanted tissue-engineered muscular urethras. *Biomaterials.* 2014;35:105-12.
- Inatomi T, Nakamura T, Kojyo M, Koizumi N, Sotozono C, Kinoshita S. Ocular surface reconstruction with combination of cultivated autologous oral mucosal epithelial transplantation and penetrating keratoplasty. *Am J Ophthalmol.* 2006;142:757-64.
- Babič M, Horák D, Trchová M, Jendelová P, Glogarová K, Lesný P, et al. Poly(L-lysine)-modified iron oxide nanoparticles for stem cell labeling. *Bioconjug Chem.* 2008;19:740-50.
- Jasmin, Torres A-L-M, Nunes H-M-P, Passipieri J-A, Jelicks L-A, Gasparetto E-L, et al. Optimized labeling of bone marrow mesenchymal cells with superparamagnetic iron oxide nanoparticles and in vivo visualization by magnetic resonance imaging. *J Nanobiotechnology.* 2011;9:4.
- Cohen M-E, Muja N, Feinstein N, Bulte J-W, Ben-Hur T. Conserved fate and function of ferumoxides-labeled neural precursor cells in vitro and in vivo. *J Neurosci Res.* 2010;88:936-44.
- Yin T, Huang P, Gao G, Shapter J-G, Shen Y, Sun R, et al. Superparamagnetic Fe₃O₄-PEG2K-FA@Ce6 Nanoprobes for in Vivo Dual-mode Imaging and Targeted Photodynamic Therapy. *Sci Rep.* 2016;6:36187.
- Wang C, Xu J, Wang J, Rong Z, Li P, Xiao R, et al. Polyethylenimine-interlayered silver-shell magnetic-core microspheres as multifunctional SERS substrates. *J Mater Chem C.* 2015;3:8684-93.
- Dorin R-P, Pohl H-G, De Filippo R-E, Yoo J-J, Atala A. Tubularized urethral replacement with unseeded matrices: what is the maximum distance for normal tissue regeneration? *World J Urol.* 2008;26:323-6.
- Fu Q, Deng CL, Song X-F, Xu Y-M. Long-term study of male rabbit urethral mucosa reconstruction using epidermal cell. *Asian J Androl.* 2008;10:719-22.
- Orabi H, AbouShwareb T, Zhang Y, Yoo J-J, Atala A. Cell-seeded tubularized scaffolds for reconstruction of long urethral defects: a preclinical study. *Eur Urol.* 2013;63:531-8.
- Li H, Xu Y, Xie H, Li C, Song L, Feng C, et al. Epithelial-differentiated adipose-derived stem cells seeded bladder acellular matrix grafts for urethral reconstruction: an animal model. *Tissue Eng Part A.* 2014;20:774-84.
- Li C-L, Liao W-B, Yang S-X, Song C, Li Y-W, Xiong Y-H, et al. Urethral Reconstruction Using Bone Marrow Mesenchymal Stem Cell- and Smooth Muscle Cell-Seeded Bladder Acellular Matrix. *Transplant Proc.* 2013;45:3402-7.
- Fu Q, Deng C-L, Liu W, Cao Y-L. Urethral replacement using epidermal cell-seeded tubular acellular bladder collagen matrix. *BJU Int.* 2007;99:1162-5.
- Xie M, Xu Y, Song L, Wang J, Lv X, Zhang Y. Tissue-engineered buccal mucosa using silk fibroin matrices for urethral reconstruction in a canine model. *J Surg Res.* 2014;188:1-7.
- Guo H, Sa Y, Huang J, Wang Z, Wang L, Xie M, et al. Urethral Reconstruction with Small Intestinal Submucosa Seeded with Oral Keratinocytes and TIMP-1 siRNA Transfected Fibroblasts in a Rabbit Model. *Urol Int.* 2015;96:223-30.
- Feng C, Xu Y-m, Fu Q, Zhu W-d, Cui L. Reconstruction of Three-Dimensional Neourethra Using Lingual Keratinocytes and Corporal Smooth Muscle Cells Seeded Acellular Corporal Spongiosum. *Tissue Eng Part A.* 2011;17:3011-9.
- Hodde J-P, Record R-D, Liang H-A, Badylak S-F. Vascular endothelial growth factor in porcine-derived extracellular matrix. *Endothelium.* 2001;8:11-24.
- Mikami H, Kuwahara G, Nakamura N, Yamato M, Tanaka M, Kodama S. Two-layer tissue engineered urethra using oral epithelial and muscle derived cells. *J Urol.* 2012;187:1882-9.
- Zorlutuna P, Elsheikh A, Hasirci V. Nanopatterning of Collagen Scaffolds Improve the Mechanical Properties of Tissue Engineered Vascular Grafts. *Biomacromolecules.* 2009;10:814-21.
- Stephens P, Davies K-J, Ocleston N, Pless R-D, Kon C, Daniels J, et al. Skin and oral fibroblasts exhibit phenotypic differences in extracellular matrix

- reorganization and matrix metalloproteinase activity. *Br J Dermatol.* 2001;144:229-37.
- [41] Peng L, Jia Z, Yin X, Zhang X, Liu Y, Chen P, et al. Comparative analysis of mesenchymal stem cells from bone marrow, cartilage, and adipose tissue. *Stem Cells Dev.* 2008;17:761-73.
- [42] Huri P-Y. Effect of Culture Conditions on the Multinucleation of Human Adipose-Derived Stem Cells. *J Biomater Tissue Eng.* 2015;5:234-40.
- [43] Tan S-J, Fang J-Y, Wu Y, Yang Z, Liang G, Han B. Muscle tissue engineering and regeneration through epigenetic reprogramming and scaffold manipulation. *Sci Rep.* 2015;5:16333.
- [44] Shimizu T, Sekine H, Yang J, Isoi Y, Yamato M, Kikuchi A, et al. Polysurgery of cell sheet grafts overcomes diffusion limits to produce thick, vascularized myocardial tissues. *FASEB J.* 2006;20:708-10.
- [45] Siemerink M-J, Klaassen I, Vogels I-M-C, Griffioen A-W, Van Noorden C-J-F, Schlingemann R-O. CD34 marks angiogenic tip cells in human vascular endothelial cell cultures. *Angiogenesis.* 2012;15:151-63.
- [46] Sekiya S, Shimizu T, Yamato M, Kikuchi A, Okano T. Bioengineered cardiac cell sheet grafts have intrinsic angiogenic potential. *Biochem Biophys Res Commun.* 2006;341:573-82.
- [47] Sekine H, Shimizu T, Hobo K, Sekiya S, Yang J, Yamato M, et al. Endothelial Cell Coculture Within Tissue-Engineered Cardiomyocyte Sheets Enhances Neovascularization and Improves Cardiac Function of Ischemic Hearts. *Circulation.* 2008;118:S145-S52.
- [48] Ren L, Kang Y, Browne C, Bishop J, Yang Y. Fabrication, vascularization and osteogenic properties of a novel synthetic biomimetic induced membrane for the treatment of large bone defects. *Bone.* 2014;64:173-82.
- [49] Neri M, Maderna C, Cavazzin C, Deidda-Vigoriti V, Politi LS, Scotti G, et al. Efficient in vitro labeling of human neural precursor cells with superparamagnetic iron oxide particles: relevance for in vivo cell tracking. *Stem Cells.* 2008;26:505-16.
- [50] Guzman R, Uchida N, Bliss T-M, He D, Christopherson K-K, Stellwagen D, et al. Long-term monitoring of transplanted human neural stem cells in developmental and pathological contexts with MRI. *Proc Natl Acad Sci U S A.* 2007;104:10211-6.
- [51] Sievert K-D, Selent-Stier C, Wiedemann J, Greiner T-O, Amend B, Stenzl A, et al. Introducing a large animal model to create urethral stricture similar to human stricture disease: a comparative experimental microscopic study. *J Urol.* 2012;187:1101-9.
- [52] Sangkum P, Gokce A, Tan R-B, Bouljihad M, Kim H, Mandava S-H, et al. Transforming Growth Factor-beta1 Induced Urethral Fibrosis in a Rat Model. *J Urol.* 2015;194:820-7.
- [53] Chang I-Y, Kim J-N, Kim S-O, Han M, Huh J-S, Maeng Y-H, et al. Morphological effects of mitomycin C on urothelial responses to experimentally-induced urethral stricture in rats. *Int J Urol.* 2015;22:702-9.
- [54] Xu Y-M, Fu Q, Sa Y-L, Zhang J, Song L-J, Feng C. Outcome of small intestinal submucosa graft for repair of anterior urethral strictures. *Int J Urol.* 2013;20:622-9.
- [55] Fiala R, Vidlar A, Vrtal R, Belej K, Student V. Porcine small intestinal submucosa graft for repair of anterior urethral strictures. *Eur Urol.* 2007;51:1702-8; discussion 8.
- [56] Patterson J-M, Chapple C-R. Surgical techniques in substitution urethroplasty using buccal mucosa for the treatment of anterior urethral strictures. *Eur Urol.* 2008;53:1162-71.
- [57] Rosenbaum C-M, Schmid M, Ludwig T-A, Kluth L-A, Dahlem R, Fisch M, et al. Redo buccal mucosa graft urethroplasty: success rate, oral morbidity and functional outcomes. *BJU Int.* 2016;118:797-803.